International Journal of Multiphase Flow 194 (2026) 105488

Contents lists available at ScienceDirect

International Journal of Multiphase Flow

journal homepage: www.elsevier.com/locate/ijmulflow

Oil droplet from blowouts: Role of gas and dispersant

Ruixue Liu [a], Subhamoy Gupta [b], Cosan Daskiran [c], Changyang Tan [b], Diego Muriel [b], Joseph Katz [b], Zhaonian Qu [a], Kenneth Lee [d], Michel Boufadel [a,*]

[a] *Center for Natural Resources, Civil and Environmental Engineering Department, New Jersey Institute of Technology, Newark, NJ 07102, USA*
[b] *Department of Mechanical Engineering, Johns Hopkins University, Baltimore, MD 21218, USA*
[c] *Department of Mechanical Engineering, State University of New York at Binghamton, Binghamton, NY 13902, USA*
[d] *Kenneth Lee Research Inc., Halifax, Nova Scotia B3H 4H4, Canada*

ARTICLE INFO

Keywords:
Underwater oil jet
Oil droplet size distribution
Churn flow
Dispersant

ABSTRACT

Oil and gas often emanate jointly during a subsea oil blowout. Based on the proportions of the two phases, the hydraulic regime within the pipe could be bubbly, churn, slug, annular, and dispersed. We hypothesized herein that the regime impacts the oil droplet size distribution (DSD) in the blowout in the absence and presence of chemical dispersant (essentially surfactant). In this paper, we conducted oil and air jet releases in a 0.6 m diameter, and 2.6 m vertical water tank. The results showed that the churn flow caused a decrease of oil droplet sizes under the condition of same effective momentum, demonstrating that extra turbulence was introduced in the flow compared to bubbly flow. The application of dispersant significantly decreased the droplet sizes for both oil-only flow and oil-air jets. The phenomena of compound droplets were also identified for both oil only jets and oil-air jets. Generally, this work can contribute both experimental benchmarks for model validation and practical guidance for optimizing response decisions during deepwater oil spill events.

1. Introduction

The Deepwater Horizon (DWH) oil spill was a catastrophe to the environment, where approximately 900,000 tons of crude oil and up to 170,000 tons of gaseous hydrocarbons were released into the Gulf of Mexico of 1500 m (Gros et al., 2017; Reddy et al., 2012). The released hydrocarbons proceeded through the water column to the surface and subsequently to the shorelines (Boufadel et al., 2022; Geng et al., 2021; Kulkarni et al., 2024). It caused adverse impacts on the ecosystem it encountered, such as the water column (Paul et al., 2013), the sea surface (Teal and Howarth, 1984), and the shorelines (Olita et al., 2012).

The release of oil and gas posed scientific challenges as there were no studies on the multiphase release of jets and plumes in water. Most of the experience was on the behavior of miscible plumes (water in water or air in air) (Fischer et al., 1979; Friehe et al., 1971), or liquid in air in the context of combustion (Gorokhovski and Herrmann, 2008; Reitz and Bracco, 1982). Regardless of the plume dynamics, the size of the oil droplet is critical for its fate and transport in the water column. In the Deepwater Horizon, released at 1500 m depth, large oil droplets (millimeters) rose within hours to the surface whereas small oil droplets get entrained in the intrusion zone (Gros et al., 2020; Socolofsky et al., 2011). Small droplets have also a large oil-water surface area which increases their dissolution and biodegradation rates (Viveros et al., 2015). Therefore, knowing the oil DSD is critical for determining the transport and fate of oil.

Experimental investigations have been conducted to study the oil droplet size under the release of oil-only jets (Brandvik et al., 2013; Liu et al., 2022; Masutani and Adams, 2000; Xue and Katz, 2019). Yet, experiments containing the gas phase, which results in a three-phase jet (water, oil, and gas), are rare. The DeepSpill experiment conducted in the Norwegian Sea for oil and gas release reported the size distribution within a depth range of 836–760 m (about 9–85 m above the source) (Johansen et al., 2001). However, there were large uncertainty in the measurement of the oil DSD. Malone et al. (2018) used a high-pressure laboratory setup for multi-phase (liquid and gas) hydrocarbon jets. The facility contained an inner vessel with height of 0.6 m and diameter of 0.19 m; the releasing orifice was 1.5 mm for both dead oil and live oil (oil containing dissolved gas) experiments under high pressure. The main contribution of their experiments is that they simulated the high pressure inside the vessel (161 bar) and found that a rapid degassing, due to the presence of an orifice (i.e., a constriction), can alter the oil DSD. But the pipe diameter (1.5 mm) was too small to capture the

* Corresponding author.
E-mail address: boufadel@gmail.com (M. Boufadel).

https://doi.org/10.1016/j.ijmultiphaseflow.2025.105488
Received 19 July 2025; Received in revised form 2 October 2025; Accepted 14 October 2025
Available online 15 October 2025

hydraulic regimes in the pipe (discussed next). Brandvik et al. (2019a; 2019b) released the live and dead oil under water. Their experiment showed no significant difference in oil droplet sizes versus pressure (from 5 m to 1750 m) for live oil. For the combined releases of live oil and natural gas, oil droplet sizes showed a clear reduction as a function of increased gas fraction and a weak reduction with increased depth. The latter was attributed to the increased gas density and subsequently momentum of the gas, as the experiments were conducted by conserving the volume ratios.

For pipes containing a gas phase, five regimes are usually determined (Hewitt, 2012; Montoya et al., 2013). They are: bubbly, slug, churn, annular flow, and dispersed flows (Fig. 1).

Churn flow appears as a highly oscillatory liquid film accompanied by a continuous gas core with a considerable amount of entrained liquid in the wake region. The structures are spiraling, transient and vortex-like which move throughout the system (Vermeer and Krishna, 1981). The bubbly flow and the annual flow are considerably easy to identify, yet the transition between slug flow and churn flow is more complicated. In a large pipe (D_0>0.1 m), the sufficient radial room allows the coalescence of large bubbles and results in the bubble instability and the further chaotic breakup, which is the main character of churn flow. Also in the large pipe, it is possible that the flow directly transits from bubbly flow to churn flow. On the other hand, in the small pipe, along with the increase of gas void fraction, the flow commonly evolves to slug flow. After that, the breakdown of the Taylor bubble (the main bubble) in the slug flow is believed to be caused by the rapid increase in the pressure gradient due to the intense wave activity and friction (Hewitt, 1985; Montoya et al., 2016). Churn flow/slug is believed to have occurred in the DWH riser prior to the release to sea (Boufadel et al., 2018). Van Nimwegen et al. (2015a) conducted observations of churn flow using high speed cameras. They studied the morphology, the liquid holdup, and the pressure gradient of the flow, the diameter especially under the effect of surfactants (Van Nimwegen et al., 2015b; 2017). Similarly, the observation of the film slickness at the wall when churn flow happened was made by Sharaf et al. (2016). The effect of liquid viscosity was investigated by Parsi et al. (2015). Wang et al. (2017) measured the water droplet size distribution in the churn flow happening in a 19 mm pipe. They argued that the generation of liquid droplets could result from three main mechanisms: The breakdown of liquid slug, the bag breakup, and the ligament breakup. Bag breakup dominates the formation process when the flow experiences the transition from slug flow to churn flow, while the last mechanism governs breakup when the flow is close to annular flow. Also, Wang et al. (2020), and Cao et al. (2022) studies the droplets in pipes with varied diameter where the flow ranged from the churn to annual regime. A detailed review on the liquid droplet size distribution within the pipe under annular flow is provided by Berna et al. (2015), and discussed in the Discussion section. The entrainment of oil in annular flow decreases with the gas flow until reaching zero in churn/slug flow. Of course, this does not mean that no oil droplets will exist in the gas phase of churn flow, but the total volume of these droplets is small, and thus negligible with respect to the liquid flow. Therefore, the main breakup mechanism of the oil droplets in our experiments is due to the velocity difference between water and oil, i.e., Kevin-Helmholtz instability rather than the Rayleigh-Taylor instability of oil droplets in the gas phase (i.e., due to difference in fluid densities).

However, only a few studies investigated the release of multiphase plumes in surrounding liquids. In particular, namely Iguchi et al. (1997;1995) investigated the release of water plumes with air into a body of water and evaluated the gas bubble size distribution and the jet hydrodynamics under bubbly and churn flow conditions. But to our knowledge, there was no study of liquid droplets from a churn flow released in a surrounding liquid.

In order to capture oil droplet sizes in the subsurface blowouts, here we conducted an experimental study of releasing oil and air from a pipe with 10 mm diameter in a 2.6 m height water tank. Both oil-only jet and oil-air jet were conducted, and different flow rates were selected to make the single-phase jets fall in the atomization regime (Fig. 4, discussed later) (Johansen et al., 2013). In addition, the oil-air jets hydrodynamics included the situations of churn/slug flow regime. In some experiments, the dispersant (Corexit 9500) was applied to the oil, as dispersant was used in the Deepwater Horizon spill to reduce the size of the rising oil droplets. Our goal herein was to evaluate the effectiveness of the dispersant in the presence of air.

The oil droplet sizes were measured using the shadowgraph camera and LISST-200x (described below). The results are expected to help better understand and predict the oil droplet sizes and therefore further fate and transport during subsea oil blowouts.

2. Materials and methods

2.1. Experimental setup

The multiphase jets were released in a 2.6 m height water tank located in Johns Hopkins University. The tank is composed of two vertical modules each 40 inches (around 1.0 m) in height, used in the current study. The bottom of the tank is 30 cm above the ground, allowing for the modification of the injection pipeline system. The lower 30 cm of the tank allows the full development of the jet and the installation of honeycomb materials which allows the homogeneous mixing of the continuous phase (water). The injection point was set at 60 cm above the tank-bottom. On the bottom of the tank, four water inlets were used to pump 8LPM water in total to minimize the return flow due to water entrainment by the jet. The entrained flow can be up to 100 times the released oil rate, and thus there would invariably be water that comes from the upper portion of the tank to satisfy the momentum requirement of the jet. By pumping water from below the jet, the return flow is reduced.

Four acrylic windows were constructed on each module together with 12 sampling points. As the sampling instruments (shadowgraph camera and LISST) were wider than the tank width, two main holes were manufactured at the glass to accommodate the instruments. The two apertures are positioned at 2.16 m and 2.36 m above the base for the

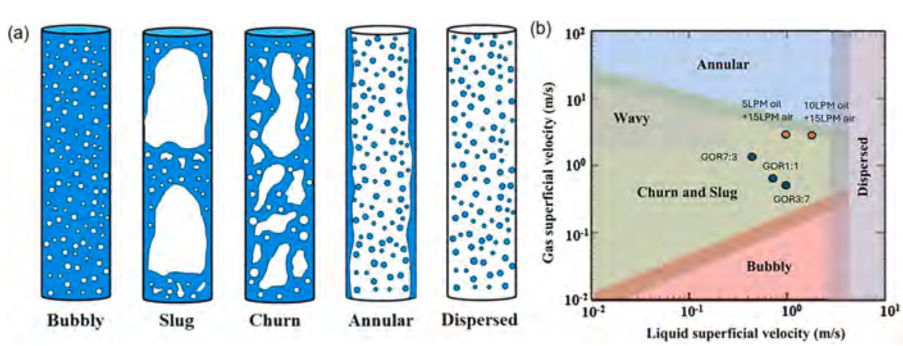

Fig. 1. (a) Hydrodynamic (or mixing) regimes for two phase flows in a vertical pipe. (b) the flow "map" from a diameter 0.10 m from (Boufadel et al., 2018).

shadowgraph camera and the LISST, respectively. One of these apertures is visible in Fig, 2b through the upper window. Given the overall height of the pipeline, the vertical distances between the jet exit and the measurement locations are 1.56 m and 1.76 m, corresponding to 156 D and 176 D for a 10 mm orifice. These distances indicate that the flow is sufficiently developed and well diluted prior to measurement. The sketch and the picture of the tank were shown in Fig. 2. The entire setup is shown in Fig. 3, including the experiment tank, the jet supply (oil, air and dispersant), the water supply, and the drainage system.

In the experiments, diesel fuel with pink dye was released through a vertical pipe into the test tank. The diesel and dispersant were stored in the pressurized storage cylinder and then released under the pressure of nitrogen. The pressure of the nitrogen tank (Airgas Inc.) was controlled and monitored by nitrogen regulators. The air was released directly from the air cylinder and was monitored by the air pressure regulator. On/Off valves were installed together with the check valves to prevent the backflow. The flow-adjustment valves were installed to manage the flow rate where the flow rates were indicated by flow meters. Artificial sea water was also released together with the oil through the water pump to ensure adequate entrainment of the jet. After the experiment, absorbent sheets were applied to remove the surface diesel. The remaining diesel was removed through the activated carbon system.

For each experiment, the system was operated for 2–5 minutes, with a 20-second sampling interval selected during a stable period. The shadowgraph camera, with a pixel size of 13.3 μm, provided reliable resolution for droplets larger than 100 μm (approximately 7.5 pixels), while smaller droplets were excluded to ensure accuracy. A focused window of 800 × 800 pixels (10.6 × 10.6 mm) was analyzed, within which most oil droplets were well captured. Images were processed using ImageJ which included background subtraction, binary conversion, hole filling, watershed segmentation, and particle analysis, ensuring consistent characterization of droplet distributions (Liu et al., 2021). The entire process was recorded as macro commands in ImageJ, enabling automatic batch processing of images. For this experiment, the same approach was applied, as outlined below for Case 1 (5 LPM oil). Although this procedure may omit some small droplets encapsulated within larger ones, their contribution to the overall distribution and to the d_{50} is limited due to their small volume. Air bubbles and major artifacts were also removed manually. The LISST-200X measures droplet sizes between 1 μm and 500 μm, which represents the typical range of dispersed oil droplets under effective dispersant application. The accuracy of LISST data is commonly assessed using the transmission value, defined as the fraction of incident light passing through the sampling chamber. Lower transmission indicates higher oil concentrations, and a minimum threshold of 30 % is applied to exclude unreliable measurements.

The interfacial tension (IFT) between diesel and artificial seawater was measured by a tensiometer (KRUSS, K20) using the Wilhelmy plate method. The plate was immersed in the diesel while slightly touching the interface between the heavy (seawater) and the light (diesel) phases. The ambient room temperature was about 22°C when conducting the measurements. The measurements were conducted in duplicate. The IFT between seawater and diesel was found to be 12.4 ± 0.237 mN/m. For a dispersant-to-oil ratio (DOR) of 1:200, which is similar to what was used in the Deepwater Horizon (Lee, 2012), the IFT decreased to 0.43 ± 0.039 mN/m. The interfacial tension between artificial seawater and air was 73.9 mN/m ± 0.007, which is slightly higher than that of freshwater (72.8 mN/m) due to water salinity (35 g/L). The surface tension between seawater and air in the presence of dispersant was taken as 35 mN/m, which is based on the study of Asari and Hormozi (2014), along with Beneventi et al. (2001) and Dey et al. (1997).

2.2. The test matrix

A total of 22 runs were conducted to evaluate the impact of air and/or dispersant. These were selected based on the values of three dimensionless groups, the Weber, Reynolds, and Ohnesorge numbers:

$$\mathrm{We} = \frac{\rho_o U_0^2 D}{\sigma_{o-w}} \quad \mathrm{Re} = \frac{\rho_o U_0^2 D}{\mu_o} \quad \mathrm{Oh} = \frac{\mu_o}{\sqrt{\rho_o \sigma_{o-w} D}} \tag{1}$$

Where ρ_o is the density of the liquid dispersed phase (oil herein); μ_o is the viscosity of oil and σ_{o-w} is the interfacial tension between oil and

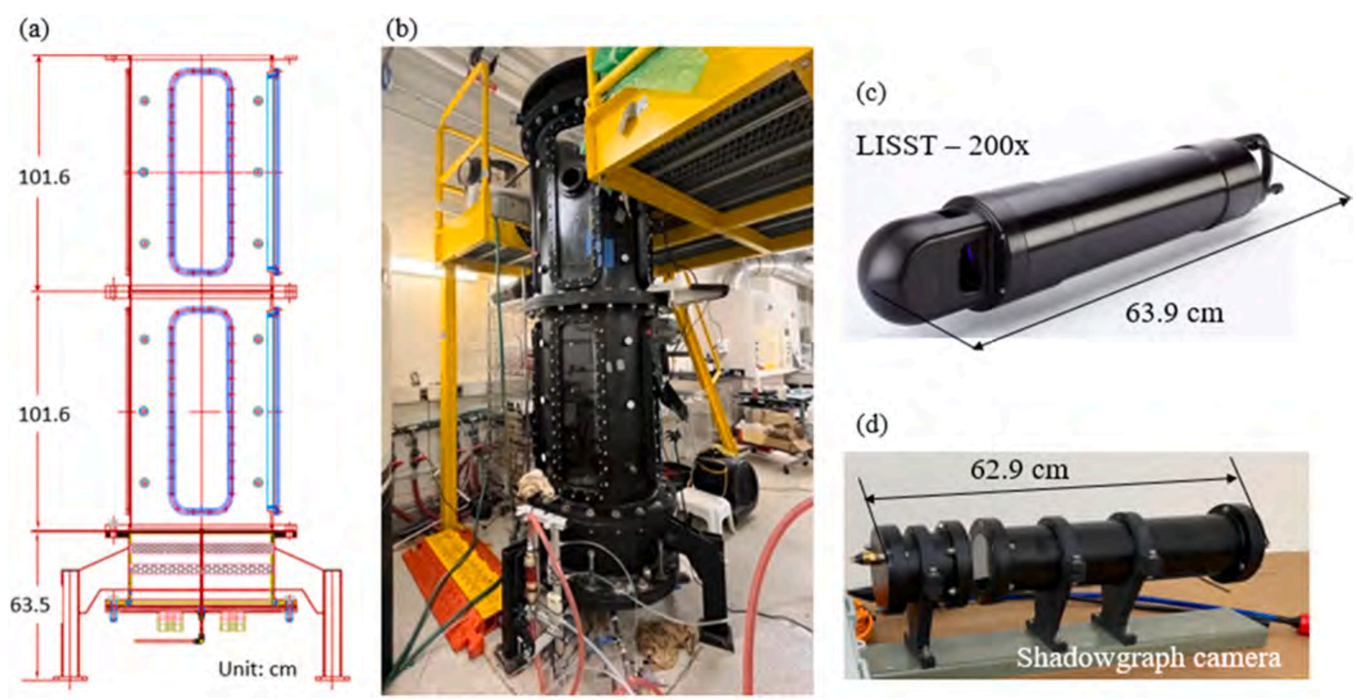

Fig. 2. The main experimental facilities and instruments: (a)-(b) the drawing and the image of the water tank (height of 2.6 m and diameter of 0.6 m); (c) the laser diffraction particle size analyzer (LISST – 200x) for measuring particles within diameter of 1 to 500 μm; (d) the shadowgraph camera for measuring particles within diameter of 10 μm to 4 cm.

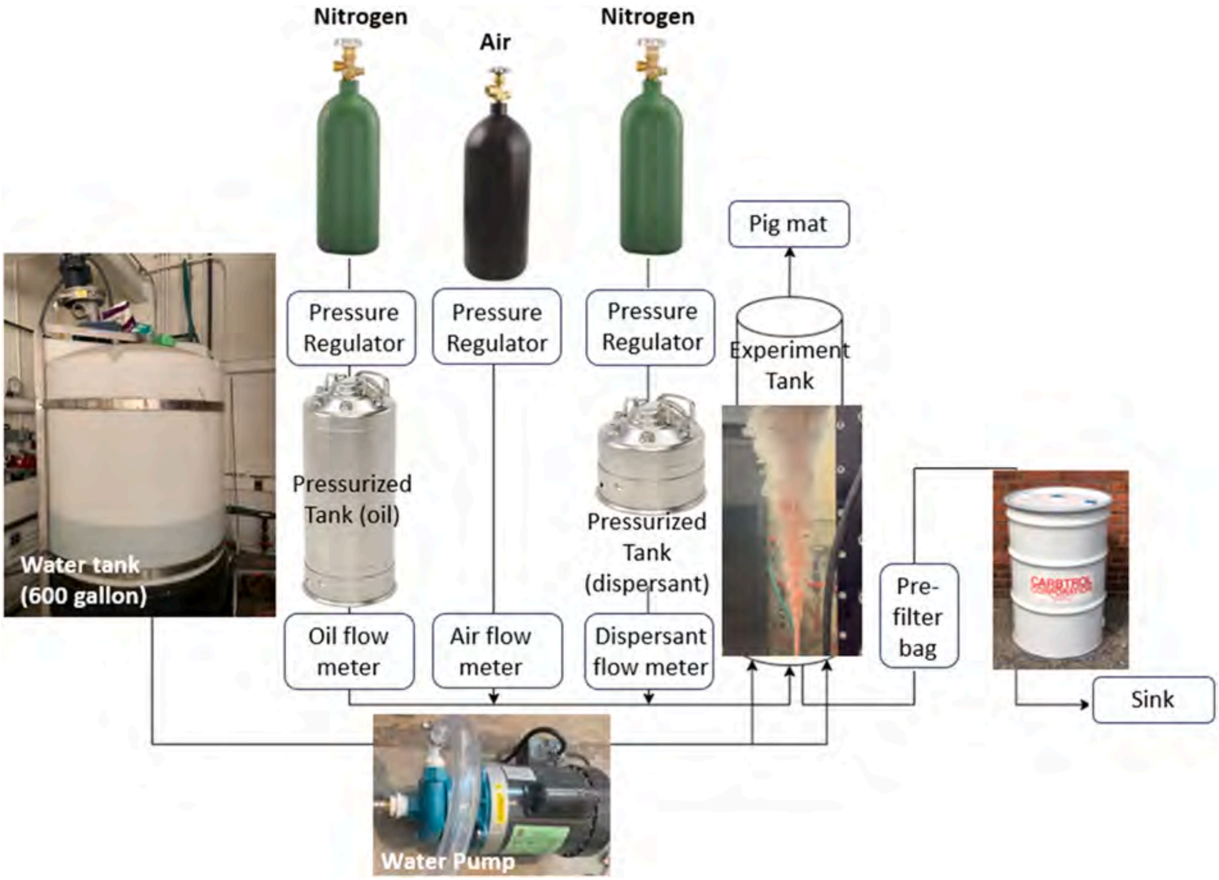

Fig. 3. The schematics of the experiment setup, including the experiment tank, the jet supply (oil, air and dispersant), the water supply, and the drainage system.

water (continuous phase);U_0 is the outlet velocity; D is the characteristic length, adopted here as the diameter of the injection pipeline. Note based on Eq. (1) that knowledge of two numbers provides the third.

The pipe diameter was 10 mm. The oil flow rates for each pipe were determined based on the Oh vs. Re number diagram (Johansen et al., 2013; Zhao et al., 2015) to make sure the jet flow is in the atomization breakup regime (Fig. 4). Based on Fig. 4, atomization required a minimum flow rate of 4.7 liters per minute (LPM) for the 10 mm pipe diameter. Therefore, 5 LPM and 10 LPM oil flow rates were adopted for the 10 mm pipe diameter. For the dispersant-to-oil ratio (DOR) of 1:200; the updated interfacial tension was substituted in the calculation of Oh and Re numbers.

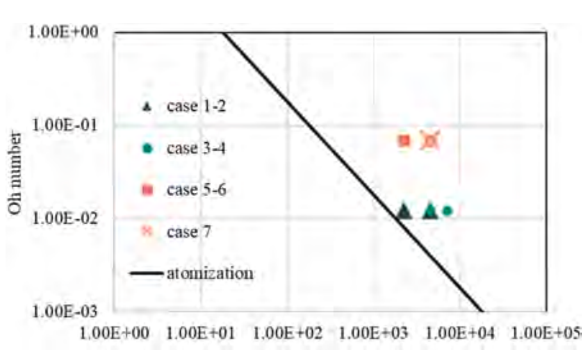

Fig. 4. The calculated Re and Oh number for Case 1 to 7 based on Eqs. (1) and 2. The black line is the line for atomization regime based on (Masutani and Adams, 2000). The effective velocity for Case 3 (5 LPM oil + 15 LPM air) is equivalent to Case 1 (10LPM oil only), which allows for a better comparison of the impact of the air phase. A similar design was adopted for Case 7 (5 LPM oil + 15 LPM air with dispersant) to Case 6 (10 LPM oil only with dispersant).

Based on the flow map (Fig. 1), the 5 LPM and 10 LPM liquid phase flow rate, the air flow rate of 15 LPM should result in the slug/churn flow regime (which was confirmed visually). Accordingly, two cases of 5 LPM oil + 15 LPM air and 10 LPM oil + 15 LPM air were decided. The Oh and Re numbers for oil-air jet were determined by calculating the equivalent effective velocity U_E, which is defined as the velocity of a single phase oil jet producing the same momentum flux as the bubbly water jet (Johansen et al., 2013; Zhao et al., 2014); and the detailed mathmatical derivation of it can be found in the Appendix A in our previous work (Zhao et al., 2014). the effective flow rate Q_E and the effective velocity U_E are calculated as:

$$Q_E = \frac{Q_o}{(1-n)^{1/2}} \tag{2a}$$

$$U_E = \frac{U_o}{(1-n)^{1/2}} \tag{2b}$$

where Q_o, U_o is the releasing flow rate and velocity of the oil phase, respectively; n is the gas void fraction determined as $n = Q_g/(Q_o + Q_g)$.

By replacing the velocity U_0 in the dimensionless numbers with the effective velocities .., the Re, Oh, and We number were computed as shown in Table 2 and Fig. 4. It should be noted that for the case of 5 LPM oil + 15 LPM air, the gas void fraction "n" is 0.75, which results in an effective velocity that is double U_o. This is equivalent to the oil only case released with the flow rate of 10 LPM.

3. Results and discussions

3.1. Jets behavior

The images of the underwater jets shown in Fig. 5 were captured from the video taken by GoPro camera from the observation window. The video file of Case 7 was corrupted, and hence no image was obtained. For Case 1 (Fig. 5(a)), the 5 LPM oil jet was near the transition region of atomization (Fig. 4). By increasing the flow rate to 10 LPM (Case 2, Fig. 5(b)), the atomization was more obvious along with the generation of smaller droplets. In both cases, the breakup is subsumed to be due to Kevin-Helmholtz (K-H) instabilities due to the shear layer between the jet/plume and the surrounding water ((Boufadel et al., 2020) and publications therein. As the plume moved downstream (i.e., upward), its cross section gradually expanded in the radial direction due to the entrainment of the surrounding water (thus it gets diluted).

For the 5 LPM oil + 15 LPM air case (Case 3, Fig. 5(c)), the flow map (Fig. 1) indicates that the plume is in the slug/churn flow. We observed visually that it was alternating between slug and churn flow. It is important to note that as the diameter of the orifice decreases, churn flow tends to get replaced by slug flow due to the size of the Taylor bubble. The air bubbles displayed intermittent behavior where the larger bubbles were only visible for brief periods of time every few seconds. Case 5 (10 LPM oil + 15 LPM air) also showed a highly chaotic turbulence, where elongated ligaments and the shredded droplets were observed at the periphery of the jet (Fig. 5(d)). Due to the collapse of the larger bubble, different patterns of air bubbles covering a wide range were observed. The unstable bubbles enhanced the mixing in the radial direction, resulting in a larger plume angle and probably larger entrainment of water.

Under the application of the dispersant, the plumes of oil-only became smoother, and the plume angle decreased. This was also noted in Gao et al. (2017). They observed that the angle of the plume without and with dispersant was around 13° and 11°, respectively. They also

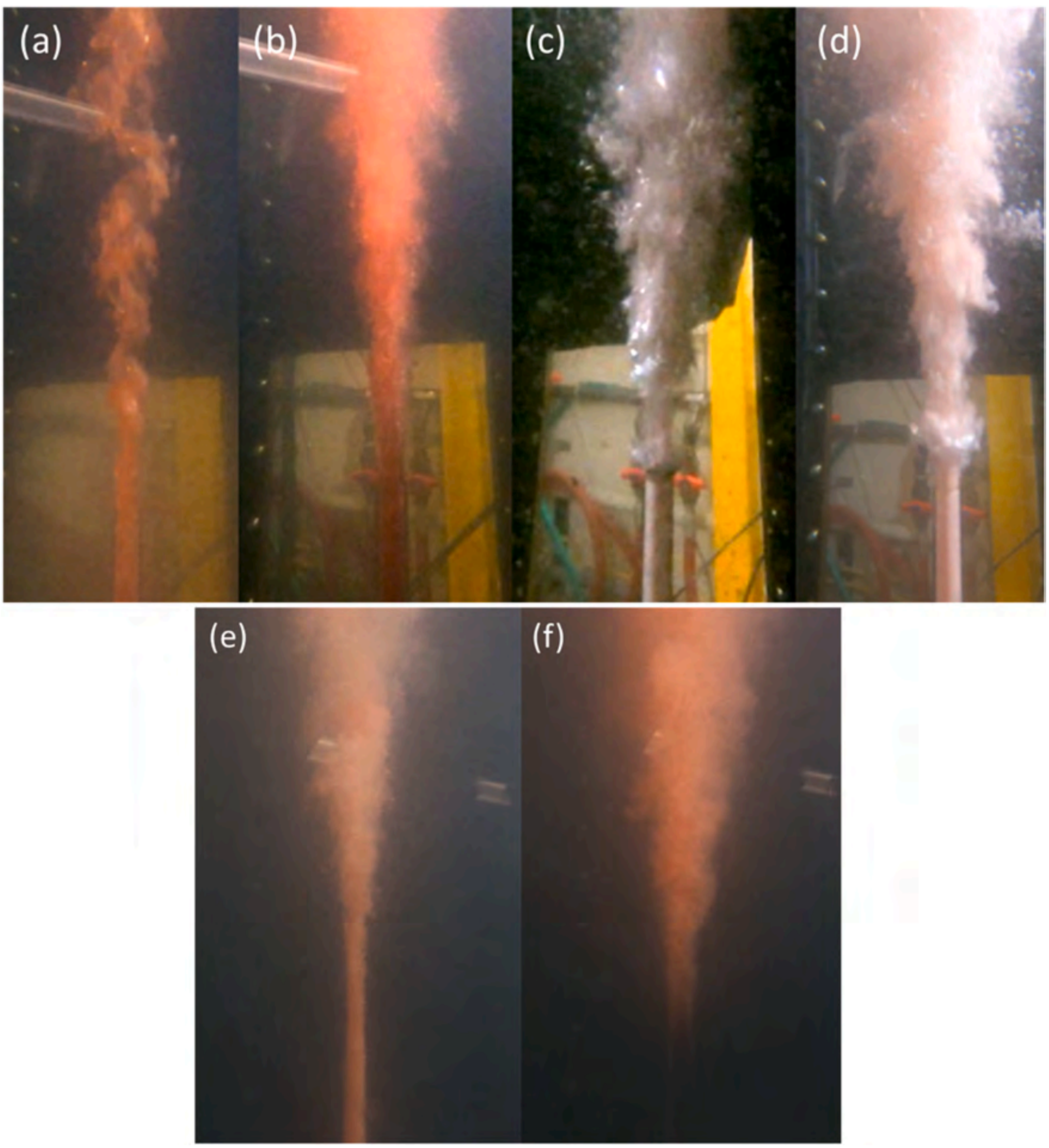

Fig. 5. The images captured by GoPro of jets from (a) Case 1 – 5 LPM oil only; (b) Case 2 – 10 LPM oil only; (c) Case 3 – 5 LPM oil + 15 LPM air; (d) Case 4 – 10 LPM oil + 15 LPM air; (e) Case 5 – 5 LPM oil only with dispersant (f) Case 6 – 10 LPM oil only with dispersant. The video file was corrupted for Case 7 (5 LPM oil + 15 LPM air with dispersant), no image was captured.